DEVELOPMENT OF ADVANCED ROCKET ENGINE TECHNOLOGY FOR PRECISION GUIDED MISSILES

Michael J. Nusca*
U.S. Army Research Laboratory
Aberdeen Proving Ground, MD 21005

R. Scott Michaels
U.S. Army Aviation and Missile Research, Development, and Engineering Center
Redstone Arsenal, AL 35898

ABSTRACT

The Army is developing hypergolic, liquid and gelled bipropellants for a small, selectable-thrust, liquid rocket engine (LRE) that can power tactical missiles for both current and future combat systems. The use of gel propellants brings the advantages of selectable thrust and the promise of small engine size but also introduces new challenges in combustion control. One of these challenges is the efficient mixing of gelled oxidizer and fuel to obtain maximum performance from the LRE combustor without increasing the size of the engine. The Army's impinging stream vortex engine, ISVE, offers an efficient alternative to increasing the combustion chamber volume of a LRE and has already generated excellent performance test data. Since the ISVE is a new concept, analytical models that relate engine performance to engine design parameters are just beginning to emerge. In order to fully exploit the performance that have been realized for the ISVE, it is desirable to understand the underlying flow physics of the engine. This paper describes the Army's effort to use multidimensional, multiphase computational fluid dynamics, combined with high-performance computers to generate simulations of the ISVE that reveal combustion patterns as well as predict chamber pressure and thrust levels for the engine. The goal is to utilize this computational tool to optimize the ISVE performance for a host of strategic Army missions.

1. INTRODUCTION

A common, modular, small, low cost precision guidance weapon is required by the Army's RDECOM and the Aviation and Missile Research Development and Engineering Center (AMRDEC) for the Army's Future Combat System (FCS). This weapon (missile system) must be capable of engaging a variety of targets with minimal collateral damage. In contrast, current lethality options being developed for the FCS are focused on defeating heavily armored targets with less emphasis on soft and lightly armored point targets. Therefore, a complementary, low cost, small diameter weapon system to engage soft targets with surgical strike precision is required for the FCS. The 2.75-inch guided rocket currently being demonstrated in the Low Cost Precision Kill (LCPK) Advanced Technology Demonstrator (ATD) and transitioning to the Advanced Precision Kill Weapon System (APKWS) provides this capability but uses a large missile airframe. Some of the vehicle options for the FCS require a significantly shorter missile.

In order to directly address this need, the Army's AMRDEC and Army Research Laboratory (ARL) are currently engaged in a high-priority Strategic Technology Objective, STO, which continues until FY2007. Titled, Advanced Miniature Multi-Role Precision Guided Missile Technology (AMMPGM), this STO addresses key technologies that enable the upgraded 2.75-inch guided rocket to be significantly shortened while retaining performance. To achieve these goals, the overall missile drag must be reduced and a new, shorter boost/sustain LRE must be developed that takes advantage of the lower airframe drag while maintaining performance in terms of maximum range and lethality. The combination of a conformal optics technology for drag reduction and the new boost/sustain motor will enable the missile airframe to be shortened by the required 30% and therefore be ready for integration into the FCS spirals.

Concurrent with the above goals, such next generation missiles must have a "selectable thrust" capability. The Army has identified the need for missile systems with thrust modulation over wider ranges than those achievable with current technology. Current capabilities in controllable thrust technology require extensive modification in order to achieve increase range, enhanced end game scenarios, and multi-mission capabilities for a family of close combat weapons. Such multi-mission scenarios require a single missile with the capability to attack near-range targets, attack medium range targets via loiter and seek methodologies, and perform beyond line-of-sight (BLOS) missions via smart on-board guidance and seeker technology. Integrating these

Report Documentation Page

Form Approved
OMB No. 0704-0188

1. REPORT DATE	2. REPORT TYPE	3. DATES COVERED
00 DEC 2004	**N/A**	**-**

4. TITLE AND SUBTITLE	5a. CONTRACT NUMBER
Development Of Advanced Rocket Engine Technology For Precision Guided Missiles	5b. GRANT NUMBER
	5c. PROGRAM ELEMENT NUMBER
6. AUTHOR(S)	5d. PROJECT NUMBER
	5e. TASK NUMBER
	5f. WORK UNIT NUMBER
7. PERFORMING ORGANIZATION NAME(S) AND ADDRESS(ES) **U.S. Army Research Laboratory Aberdeen Proving Ground, MD 21005; U.S. Army Aviation and Missile Research, Development, and Engineering Center Redstone Arsenal, AL 35898**	8. PERFORMING ORGANIZATION REPORT NUMBER
9. SPONSORING/MONITORING AGENCY NAME(S) AND ADDRESS(ES)	10. SPONSOR/MONITOR'S ACRONYM(S)
	11. SPONSOR/MONITOR'S REPORT NUMBER(S)

12. DISTRIBUTION/AVAILABILITY STATEMENT
Approved for public release, distribution unlimited

13. SUPPLEMENTARY NOTES
See also ADM001736, Proceedings for the Army Science Conference (24th) Held on 29 November - 2 December 2005 in Orlando, Florida. , The original document contains color images.

14. ABSTRACT

15. SUBJECT TERMS

16. SECURITY CLASSIFICATION OF:			17. LIMITATION OF ABSTRACT	18. NUMBER OF PAGES	19a. NAME OF RESPONSIBLE PERSON
a. REPORT	b. ABSTRACT	c. THIS PAGE			
unclassified	**unclassified**	**unclassified**	**UU**	**8**	

enhanced capabilities with the advances in guidance and sensor technologies will greatly improve the weapon system performance especially in the Army's Common Missile and Net Fires programs. However, these capabilities require an adaptable and throttleable LRE as well as a propellant with the appropriate chemical/physical properties and insensitive munitions (IM) characteristics.

Research in this area has yielded gelled propellants that are simply liquid propellants with additives that increase the viscosity and other flow characteristics (Thompson et al., 1995; Thompson and Allan, 1995; Chew et al., 1998; Thompson et al., 1999). Gelled propellants have been shown to meet IM requirements while being safer than either liquid or solid propellants. In addition, the gelled propellant propulsion system can be throttled to actively change the trajectory of the missile (i.e., "selectable thrust") and at the same time gelled propellants can produce a theoretical specific impulse, ISP (thrust produced by the engine normalized by the weight of the engine's through-flow) of 275-280 seconds. The average solid propellant rocket delivers an ISP of 250 seconds or less. One such gelled oxidizer/fuel combination consists of inhibited red fuming nitric acid, IRFNA, and monomethyl hydrazine, MMH. Along with the advantages of selectable thrust, the use of gel propellants for missile propulsion introduces new challenges in flow and combustion control. Due to increases in chamber pressure and reduction in injector pressure, the gels pose challenges for optimal fuel/oxidizer mixing time, which must be as short as possible in order to obtain maximum performance from the combustor. This challenge is intensified by the introduction of carbon particulate used to enhance the density impulse of the propellant system. For conventional LREs, mixing difficulties are typically overcome by increasing the combustion chamber volume with a corresponding increase in engine weight – an option that is not acceptable in the AMMPGM STO or for the FCS program.

The impinging stream vortex engine, ISVE (Michaels and Wilson, 1995; Wilson and Connaughton, 1967) that is being developed at AMRDEC, offers an alternative to increasing the length and volume of conventional LRE combustion chambers. The AMRDEC ISVE, shown schematically in Figure 1, is radically different from the conventional impinging stream engine (ISE). In the AMRDEC ISVE propellants are injected tangentially to the chamber wall, impinge, and then swirl via the vortex flow that is generated by this tangential injection component. The initial mixing occurs during stream impingement and the final mixing occurs in the highly turbulent vortex region between the injector orifices and the chamber walls. There has been some evidence from post-test examination of the engine hardware that the heavier solid particles separate from the gas particles and move toward the chamber walls. It has been postulated that centrifugal movement of the solid particles increases the path length and thus increases the fluid transit time in the combustion zone. Since the efficiency of fuel/oxidizer mixing is related to this transit time, the real advantage of the ISVE is that the engine's L^* (defined as the combustor volume divided by the area of the sonic throat, that is directly proportional to the fluid transit time) can be made much smaller thereby decreasing the size and weight of the engine. An additional attribute of the vortex injection concept is that the propellants provide transpiration cooling, protecting the radial chamber wall from the combustion flame. Testing of the ISVE has yielded delivered specific impulse efficiencies of 250-255 sec for an L^* of 13 cm using IRFNA as oxidizer and 50 percent carbon-loaded MMH as the fuel. For the conventional ISE (i.e., without the vortex injection) the delivered ISP is 260-265 sec (i.e., closer to theoretical 275-280 sec) but at the cost of increasing the L^* to 25 or 50 cm, i.e., larger engine (Michaels and Wilson, 1995).

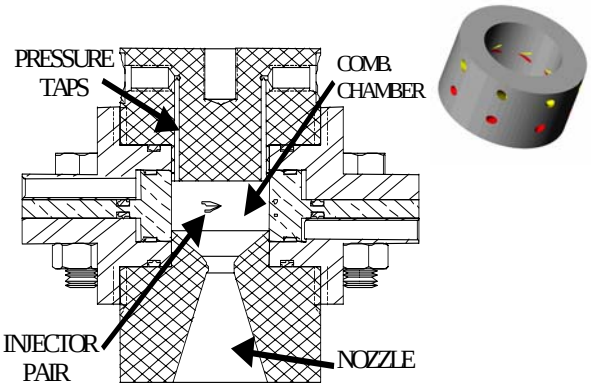

Figure 1. Schematic of the ISVE in an engine test block.

Since the ISVE is a relatively new concept, the databases and analytical models relating performance to the engine design (such as size) have not been formulated. In order to fully exploit the performance advantages that have been realized for the ISVE and to optimize the engine at other scales, it is desirable to understand the underlying flow physics of the engine. In particular, the small time delay between fuel/oxidizer injection, rapid pressurization of the combustion chamber, and chamber wall cooling are important features. To address these issues, a cooperative effort was initiated between the Propulsion and Structures Directorate of AMRDEC and the Weapons and Materials Research Directorate of the ARL.

Computational modeling of the ISVE is being conducted at the ARL using the ARL-NSRG3 code. This code is a time-accurate CFD code that has been designed to simulate unsteady, multi-component, chemically reacting (nonequilibrium) flows in various gasdynamic applications (Nusca, 1998; Nusca, 2002; Nusca et al., 2002). The NSRG3 code was chosen for TRL 3-5 engine design work for the Army's AMMPGM Strategic Technology Objective. In addition, the application of the ARL-NSRG3 code to selectable thrust rocket engines was selected as a DOD High Performance Computing (HPC) Challenge Project. This project is coordinated by the DOD HPC Modernization Office and is being lead at ARL by the first author who programs and executes the ARL-NSRG3 code on DOD HPC resources in support of Army missile research and specifically the AMMPGM STO.

2. COMPUTATIONAL FLUID DYNAMICS CODE

The high-temperature, non-ideal, chemically reacting gas flow field within the ISVE is numerically simulated using CFD. The ARL-NSRG3 code was written by the first author (Nusca, 1998; Nusca, 2002; Nusca et al., 2002) to solve the 3D, unsteady, real-gas Navier-Stokes equations. Computational submodels that represent finite-rate (nonequilibrium) chemical kinetics, multi-species diffusion and thermodynamic properties (specific heats), non-Newtonian viscosity, turbulence, and droplet vaporization/decomposition are used to augment these equations. These partial differential equations are cast in conservation form and converted to algebraic equations using a finite-volume formulation. Solution takes place on a mesh of nodes distributed in a zonal fashion throughout the flow field such that sharp geometric details are accurately represented. The conservation law form of the equations assures that the end states of regions of discontinuity (e.g., shocks, and deflagrations) are physically correct even when smeared over a few computational cells.

Further details for the ARL-NSRG3 CFD code, including governing equations, computational methodology and code validation can be obtained from other sources (Nusca, 1998) and are not repeated in this paper. For application to the ISVE, the code was upgraded with routines to simulate both the gelled and multiphase (i.e., droplet) nature of the propellants as discussed below.

Gelled fluids like MMH and IRFNA exhibit non-Newtonian behavior. Chew (Chew et al., 1998) and later Rahimi (Rahimi and Natan, 2000), observed that many non-Newtonian gels obey a power-law relating the shear stress, τ, to the strain rate (γ). Further an apparent viscosity can be defined as η,

$$\tau = \mathrm{K}\left(\dot{\gamma}\right)^{\mathrm{n}} \quad ; \quad \eta = \tau\left(\dot{\gamma}\right)^{-1} = \mathrm{K}\left(\dot{\gamma}\right)^{\mathrm{n}-1} \qquad (1)$$

so that for n = 1 we have $\eta = \mu = K$. For n > 1 the fluid is shear thickening (or dilatant) and for 0 < n < 1 the fluid is shear thinning (or psuedoplastic). Typical water gel is modeled using K = 16.75 (Pa s^n) and n = .41 and RP-1/AL gel uses K = 13.5 (Pa s^n) and n = .47./ This model for the gelled propellants was incorporated into the ARL-NSRG3 CFD code (Nusca and Michaels, 2004).

In order to model the gas/droplet mixture of both fuel and oxidizer that is injected into the ISVE, a two-phase flow is assumed in which the dispersed phase is in the form of discrete single-component spherical liquid droplets with density that is much larger than the density of the ambient gas in the chamber. Miller (Miller et al., 1998) studied the effectiveness and utility of several evaporation models for "many-droplet" gas-liquid flow simulations. The present work seeks to incorporate the most effective droplet sub-model while keeping the number of parameters as small as possible and the requirement for data that is either unknown or poorly known at a minimum. Accordingly, several of the eight models described by Miller, will eventually be incorporated into the ARL-NSRG3 code and tested for application to the ISVE. Initially the first of these, the "classical rapid mixing" model, or "infinite conductivity" model was employed in the code.

The momentum exchange between the droplets and the gas is assumed to be only a function of the drag force. The thermal energy exchange between the gas and liquid phases is assumed to occur only through convection with the internal droplet vertical flow neglected. The Lagrangian equations that describe the position, velocity, temperature, and mass of each droplet have been added to the ARL-NSRG3 CFD code (Nusca and Michaels, 2004). It is assumed that the droplets are of uniform initial diameter, D = 50 μm, and temperature (300K). The density of the IRFNA droplet is 1590 kg/m^3 , the density of the MMH droplet is 880 kg/m^3, and the latent heat of evaporation is 428 kJ/kg for both the IRFNA and the MMH droplets. Refined data for these parameters is forthcoming.

3. APPLICATION TO THE ISVE

Figure 2 shows the computational grid (203 cells along the chamber axis and 200 cells across the chamber diameter) constructed in each of 180 azimuthal planes, for a total of about 7 million grid cells within the three-dimensional geometry. Note that not all grid cells in this single azimuthal plane are displayed in the figure; rather every other cell has been plotted for clarity. The combined

combustion chamber and nozzle is 7.5 cm long and 2.8 cm in diameter (the figure has not been plotted to scale). In the ISVE, fuel and oxidizer are injected into the engine through pairs of injector orifices located around the chamber's radial wall (Fig. 1). For each pair of orifices, one orifice carries fuel and the other carries oxidizer. The orifices are also slightly slanted toward each other (fuel injector at 22 degs. and the oxidizer injector at 15 degs. from the chamber wall) so that the fuel and oxidizer streams within each pair immediately impinge. In addition, the orifices are slanted slightly in the azimuthal direction (fuel injector at 45 degs. and the oxidizer injector at 20 degs. from the chamber wall) so that the impinging fuel/oxidizer streams begin with an azimuthal velocity component, i.e., swirl. The location of these injector pairs is indicated on Figure 2 by black bars (the azimuthal plane displayed cuts through two pairs of injector orifices located 180-degrees apart). The orifices are not explicitly represented in the simulation, rather fuel/oxidizer are injected into the grid cell adjacent to the chamber wall at these locations.

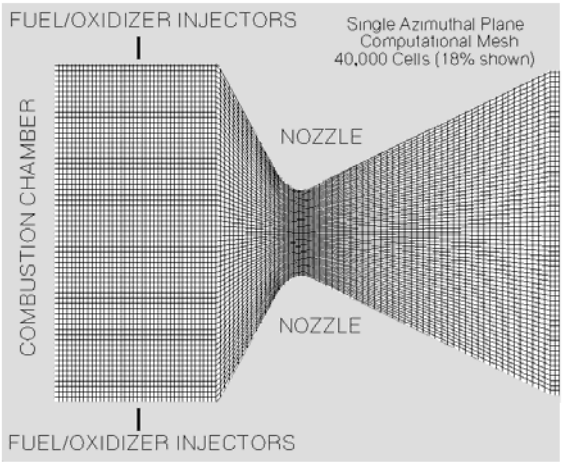

Figure 2. Computational grid for ISVE showing a single azimuthal plane containing two pairs of opposed injectors (not all cells plotted for clarity).

The particular engine design displayed in Figures 1 and 2 is designated Engine No. 1 that belongs to a family of ISVE designs being tested at the AMRDEC. A different engine design, designated Engine No. 5, has a chamber length/diameter ratio twice that of Engine No.1, an overall length/diameter of about 3.5 (2.5 for No.1) and twice as many injector pairs. In addition, Engine No. 5 has an oxidizer flow rate and a fuel flow rate which are 40% and 10% higher, respectively, as compared to Engine No. 1. In order to test the ARL-NSRG3 CFD code, results from both designs will be presented in this paper.

In practice, oxidizer alone is injected into the chamber of the ISVE until the approximate time in which fully developed (choked) flow is established in the engine. At this time, fuel is injected. During injection, the fuel and oxidizer lines are pressurized to about 2600 psia. Consequently, the prescribed initial injection rates are reduced over time by the diminishing pressure differential between these lines and the chamber (computed as part of the CFD code). At the time of injection for Engine No. 1, the oxidizer flows into the chamber at about 130 m/s and the fuel at about 190 m/s, while at the time of steady engine operation (i.e., oxidizer flow rate of .532 lb_m/s and fuel flow rate of .208 lb_m/s) these velocities have decreased to about 50 m/s and 70 m/s, respectively. The ARL-NSRG3 code was setup for just such a scenario.

At the injector orifices oxidizer and fuel gases flow with injection velocities as described above and droplets of these propellants are injected at a rate of two droplets per time step (approximately 5 μs interval). The droplets are assumed to be of uniform size and initial temperature. The simultaneous injection of both gases and droplets is consistent with the assumption that some droplet evaporation occurs within the injection system. Reliability of this assumption is being tested.

The fuel consists of MMH (CH_3NHNH_2) and the oxidizer consists of IRFNA ($H_{.8894}N_{.9635}O_{2.6989}$) or more simply nitric acid, HNO_3. Thus there are two reactants. An equilibrium analysis indicates that there are 14 major products of combustion: O_2 , N_2 , CO_2 , CO, H_2 , H, H_2O, H_2O_2 , HO_2 , HNO, NO, NO_2, O, and OH. It can be assumed that the fuel and oxidizer react in a hypergolic fashion (i.e., very fast reaction rate) when present in the specified proportions (e.g., oxidizer/fuel ratio). The stoichiometric coefficients of the product species for an assumed one-step reaction are determined using a typical execution of the NASA-Lewis equilibrium thermodynamics code (McBride and Gordon, 1986) using an oxidizer/fuel ratio of 2.6. Using this one-step reaction in the CFD code yields results that are quite sensitive to the choice of rate constants. After sensitivity analyses were conducted, a constant reaction rate of 100 moles/cm^3-sec was chosen. See Nusca (Nusca and Michaels, 2004) for further details.

Due to the lack of an industry-standard MMH reaction mechanism, a unique multi-step reaction mechanism was formulated by the ARL for MMH and HNO_3. This mechanism consists of 72 species and 489 reactions with rate data available for each reaction (Nusca and Michaels, 2004). This mechanism describes the decomposition of CH_3NHNH_2 to form CH_3NNH_2, CH_3NH, CH_2NH, CH_3NNH, CH_3NN, and CH_3NNCH_3. Subsequent reactions of these species forms NH_2, H_2, NH_3, CH_3, H,

HO_2, HNO, CH_4, H_2O_2, HCN, OH, H_2O, O, NH, H_2CN, CH_2O, CH_3O, and other species. The decomposition of HNO_3 forms NO_3, NO_2, HNO_2, OH, H, H_2O, NH_2O, and other species. The balance of the mechanism describes subsequent reactions that form additional species.

4. RESULTS

Figure 3 shows the computed pressure results (red, green and blue curves) as compared to measurements (black curves). The pressure tap is located at the chamber's closed end, called the "head-end" (see Figure 1). In the case of the experiment for Engine No. 1, the oxidizer was injected continuously from 0.35s and the chamber pressure reached about 900 psia before fuel was injected (starting from .39s) and combustion started; the final pressure level was about 1850 psia. A similar engine start scenario was used for Engine No. 5. The computations utilizing the one-step reaction (green curve) and the multi-step reaction (red curve) mechanisms are shown along with a simulation that did not permit chemical reaction (blue curve). Since chemical reactions are not occurring during the oxidizer injection phase, all of the computational results show a similar initial pressurization (i.e., 900-1000 psia) when compared to the experimental measurements. It is during this time that the engine flow is established in the chamber and through the nozzle.

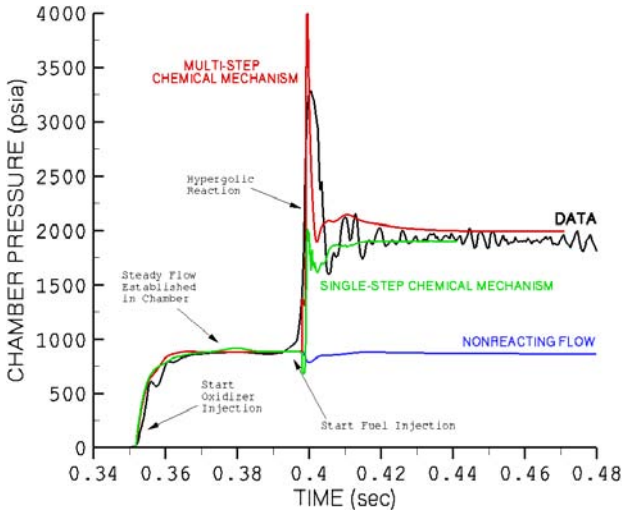

Figure 3a. Measured and computed chamber pressures for Engine No. 1.

Immediately after the time of fuel injection, the pressure measurements for both engine designs show a distinct pressure transient (i.e., pressure peak) which results from the hypergolic combustion of fuel and oxidizer. A steady engine pressure (i.e., 1800-2200 psia) with some degree of acoustic instability follows this transient. Overall, the computations that use the multi-step reaction mechanism show the best agreement with both the transient and steady-state pressures; the simulation with one-step chemistry either under or over predicts the hypergolic transient. Recall that the one-step reaction was run with a selected reaction rate chosen to achieve the best agreement with the steady pressure data (Nusca and Michaels, 2004). The multi-step reaction chemistry requires no such rate calibration. Both the measurements and the computations show that Engine No. 5 yields the higher steady chamber pressures due mainly to the increased number of injectors and propellant flow rates.

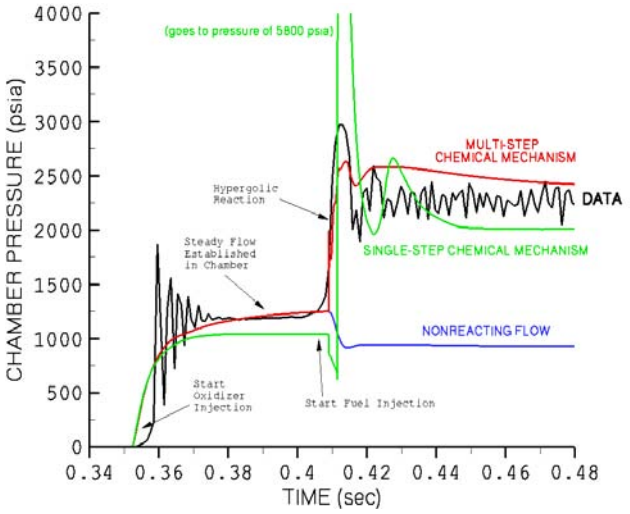

Figure 3b. Measured and computed chamber pressure for Engine No. 5.

From the results shown in Figure 3, it can be concluded: 1) the gas dynamics of the engine are represented well by the model, 2) the reaction rate for the one-step reaction was calibrated for Engine No. 1 and thus this mechanism does not perform as well for Engine No. 5, 3) the multi-step reaction mechanism does not require rate calibration and performs equally well for both engine designs, 4) the multi-step reaction mechanism captures both the transient pressure peak due to hypergolic ignition and the steady pressure level in the engines, and 5) the model does not presently contain the appropriate physics to represent the acoustic instability of the engine.

Figures 4 and 5 show pressure contours in Engine No. 1 and No. 5 for times at which the flowfield in the combustion chamber has reached a steady-state (recall Figure 3). The multi-step reaction mechanism was utilized. Injection of reactants and the stagnation of flow in the chamber have generated high-pressure regions around the

injectors and near the top of the chamber (i.e., the closed end of the chamber shown at the left in the figures). The slant of the flowfield toward the top of the chamber is caused by the strong oxidizer injection in that direction, opposed by a weaker fuel injection stream directed toward the engine nozzle. For Engine No. 5, higher pressures are realized along the centerline of the chamber at the closed end (i.e., away from the experimental pressure tap); recall that in Figure 3 the computed pressure peak for Engine No. 5 is shown as smaller than that for No. 1.

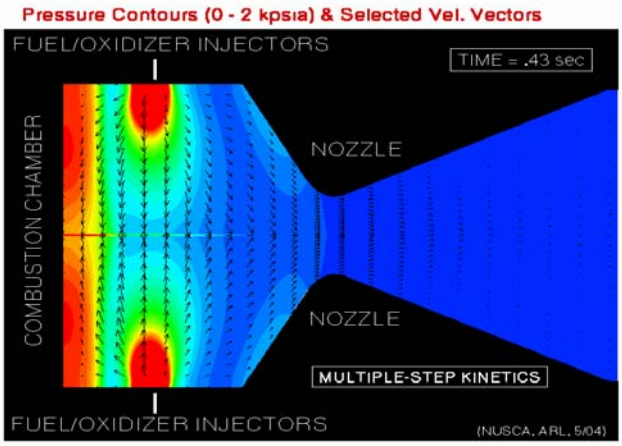

Figure 4. Computed pressure contours (blue to red: 0 to 2 kpsia) and selected velocity vectors at .43 seconds for Engine No. 1 (not to scale).

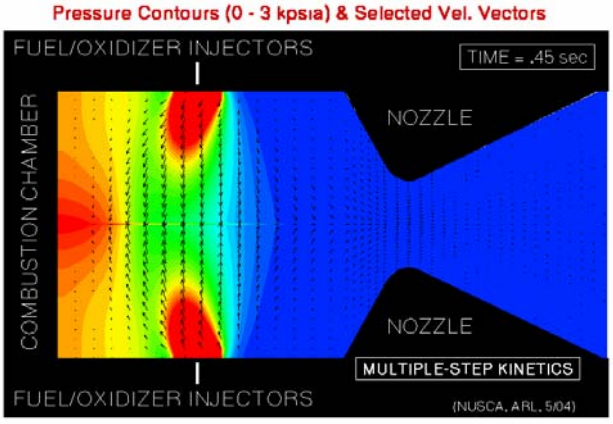

Figure 5. Computed pressure contours (blue to red: 0 to 3 kpsia) and selected velocity vectors at .45 seconds for Engine No. 5 (not to scale).

Figures 6 and 7 show contours of OH mass fraction in Engine No. 1 and No. 5 for times at which the flowfield in the combustion chamber has reached a steady-state (same times as shown in Figures 4 and 5). The multi-step reaction mechanism was utilized. The species OH is one of the most prominent reaction products and indicates the region of significant heat release in the flowfield. One notable difference in these flowfields is that most of the reaction occurs both at the injection sites and the top of the chamber for Engine No. 1 while principally at the injectors for Engine No. 5. This may be caused by the closer proximity of the injectors to the top chamber wall for Engine No. 1, which allows less time for complete combustion. The flowfields within the two engines are quite similar with subtle differences indicated in both the pressure measurements and computations (recall Figure 3).

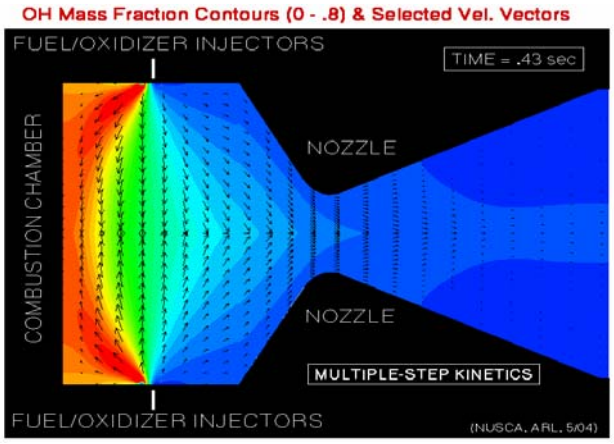

Figure 6. Computed product (OH) mass fraction contours (blue to red: 0 to .8) and selected velocity vectors at .43 seconds for Engine No. 1 (not to scale) using the multi-step mechanism.

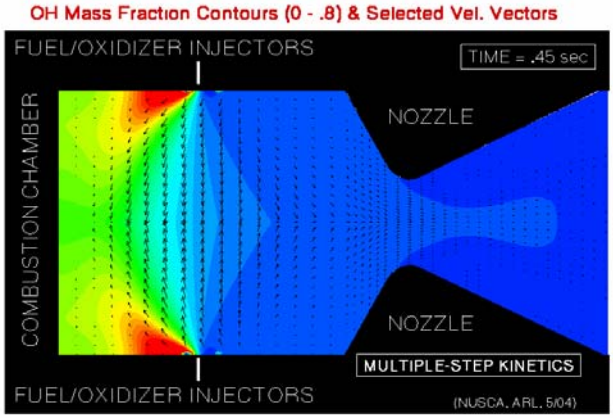

Figure 7. Computed product (OH) mass fraction contours (blue to red: 0 to .8) and selected velocity vectors at .45 seconds for Engine No. 5 (not to scale) using the multi-step mechanism.

Figures 8 and 9 show the computed OH mass fraction contours at the same times for Figures 6 and 7 but with the one-step reaction mechanism being utilized in the simulation. Note that the contour levels have been significantly reduced, relative to Figures 6 and 7, to account for the smaller amounts of OH produced using this mechanism. The one-step reaction mechanism results in major product and heat release downstream of the injectors while the multi-step reaction mechanism shows continual production of OH near the top of the chamber. A close examination of these simulations reveals that the one-step reaction produces large quantities of OH (along with other species) immediately at the injection sites and that these gases are convected toward the nozzle over time. Using these results it can be concluded that the multi-step reaction mechanism is more appropriate for simulations of the ISVE. From a computational standpoint, the multi-step mechanism requires approximately 30% more computer time per simulation.

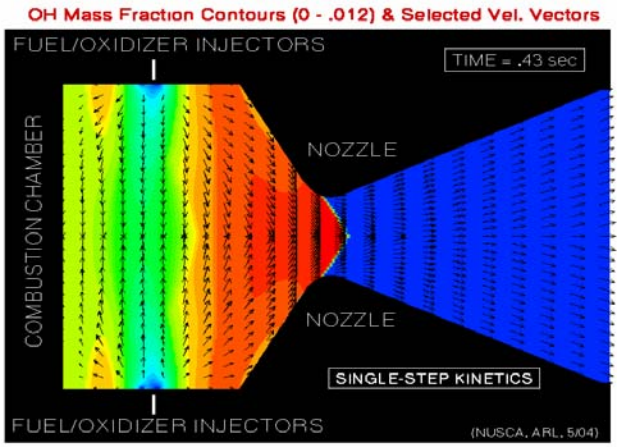

Figure 8. Computed product (OH) mass fraction contours (blue to red: 0 to .012) and selected velocity vectors at .43 seconds for Engine No. 1 (not to scale) using the single-step mechanism.

Issues related to the simulation of engine throttle, necessary for the exploration of selectable thrust options in the ISVE, have begun with a notional throttle scenario as displayed in Figure 10. Here the ARL-NSRG3 CFD code was tested to examine the physics of the re-ignition of MMH and HNO_3 which has not been widely published in the literature related to LREs. When the propellant injectors are first activated, the hypergolic pressure peak, like that shown in Figure 3, is again observed. When the injectors are momentarily shutdown and then reactivated, the chamber pressure drops but then recovers as propellants reignite. Space limitations in this paper prevent the display of computed flowfields that clearly show this event. Evidently, after a certain number of these cycles, the chamber pressure reaches an equilibrium level that is less sensitive to throttle, an important conclusion. Further work in this area, including comparison with test data is planned.

CONCLUSION

The impinging stream vortex engine, ISVE, is a compact propulsion device that uses hypergolic gelled fuel/oxidizer and a relatively new concept for injection; the ISVE has already generated excellent performance test data at AMRDEC. Computational modeling of the ISVE is being conducted using the ARL-NSRG3 code which has been used to generate simulations of the ISVE that reveal and combustion patterns and predicts chamber pressure. A one-step, fast-chemistry reaction was postulated, and it was found that for a judicious choice of reaction rate comparison between computed and measured pressures are encouraging. The use of a new 72-species, 489-step finite-rate chemical kinetics mechanism, assembled at the ARL, greatly improved the predictions of steady and transient pressure levels in the engine.

With the goal to utilize this Army computational tool to optimize the ISVE performance for a host of strategic missions, the code will continue to undergo upgrades. Modern droplet methodologies such as the Abramzon-Sirignano model and the Langmuir-Knudsen model are undergoing testing in the code. Continued testing/improvement of the rates for the new ARL finite-rate kinetics mechanism is being pursued. Finally, advanced scientific visualization is being assembled so that non-planar views of the computed flowfield may be rendered in three-dimensions.

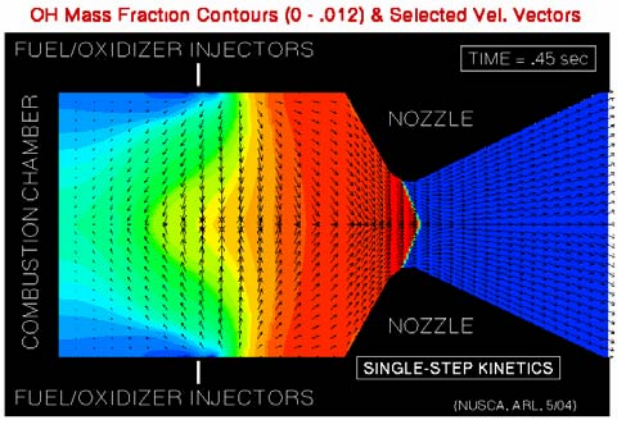

Figure 9. Computed product (OH) mass fraction contours (blue to red: 0 to .012) and selected velocity vectors at .45 seconds for Engine No. 5 (not to scale) using the single-step mechanism.

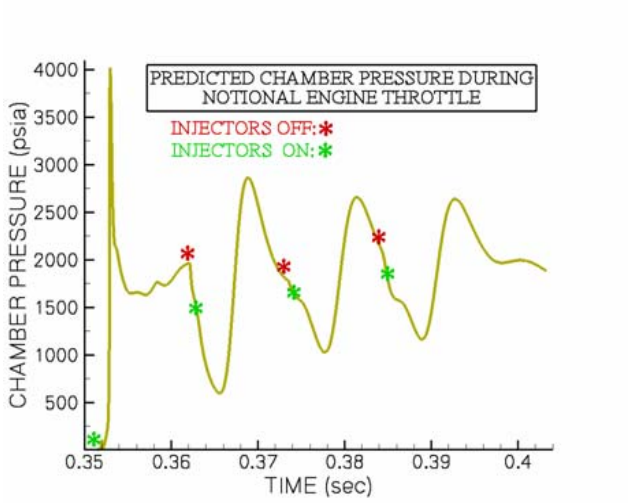

Figure 10. Computed chamber pressure for Engine No. 1 under notional throttle scenario.

ACKNOWLEDGEMENTS

Dr. Darren Thompson, Dr. Jerry Arzman, and Mr. Jon Freeman, at AMRDEC, were available for technical discussions concerning gelled propellants. The DoD Major Shared Resources Centers (ARL and NAVO) as well as Distributed Center at ARSC, supplied supercomputer time. Dr. Anthony Kotlar (ARL) formulated the one-step chemical reaction scheme used in the CFD code. Dr. William R. Anderson (ARL) formulated the multi-step chemical reaction mechanism used in the code.

REFERENCES

Chew, W.M., May, D.L., and Thompson, D.M., 1998: Non-Newtonian Rheology of Gelled Propellants, *Proceedings of the 1998 JANNAF Propulsion Meeting*, CPIA Pub. 675, **1**, 141-149.

McBride, B.J., and Gordon, S., 1986: Computer Program for Calculation of Complex Chemical Equilibrium Compositions and Applications, II. Users Manual and Program Description, NASA RP 1311.

Michaels, R.S., and Wilson, B.F., 1995: The Low L/D Vortex Engine for Gel Propulsion, *Proceedings of the 1995 JANNAF Gel Propulsion Technology Symposium*, CPIA Pub. 627, 9-16.

Miller, R.S, Harstad, K., and Bellan, J., 1998: Evaluation of Equilibrium and Non-Equilibrium Evaporation Models for Many-Droplet Gas-Liquid Flow Simulations, *International Journal of Multiphase Flow*, **24**, 1025-1055.

Nusca, M.J., 1998: Numerical Simulation of Electromagnetic Wave Attenuation in Nonequilibrium Chemically Reacting Flows, *Computers and Fluids*, **27**, 217-238.

Nusca, M.J., 2002: Numerical Simulation of the Ram Accelerator Using a New Chemical Kinetics Mechanism, *Journal of Propulsion and Power*, **18**, 44-52.

Nusca, M.J., McQuaid, M.J., and Anderson, W.R., 2002: Numerical Model of the Plasma Jet Generated by an Electrothermal-Chemical Igniter, *Journal of Thermophysics and Heat Transfer*, **16**, 44-52.

Nusca, M.J. and Michaels, R.S., 2004: Progress in the Development of a Computational Model for the Army's Impinging-Stream Vortex Engine, *Proceedings of the 40th AIAA/ASME/SAE/ASEE Joint Propulsion Conference* (AIAA Paper No. 2004-3851).

Rahimi, S., and Natan, B., 2000: Numerical Solution of the Flow of Power-Law Gel Propellants in Converging Injectors, *Propellants, Explosives, Pyrotechnics*, **25**, 203-212

Thompson, D.M., Allan, B.D., and Chew, W.M., 1995: MICOM In-House Gel Propulsion Testing, *Proceedings of the 1995 JANNAF Gel Propulsion Technology Symposium*, CPIA Pub. 627, 65-74.

Thompson, D.M., and Allan, B.D., 1995: Higher Density Impulse for Bipropellant Gel Propulsion Systems Using High Density Fuel and Oxidizer Gels, *Proceedings of the 1995 JANNAF Gel Propulsion Technology Symposium*, CPIA Pub. 627, 65-74.

Thompson, D.M., Wilson, B.F., and Stephenson, W., 1999: Hypergolic Azide Liquid Fuels, *Proceedings of the 1999 JANNAF Propellant Development and Characterization Subcommittee Meeting*, CPIA Pub. 627, 65-74.

Wilson, B.F., and Connaughton, J.W., 1967: Investigation of a Unique Design Engine Assembly, *Proceedings of the 3rd AIAA Propulsion Joint Specialist Conference*, Washington, DC.